Check for updates

Small

NANO · MICRO small
www.small-journal.com

RESEARCH ARTICLE OPEN ACCESS

Nano-Optical Biomolecular Interaction Sensing Within Complex Media via Peptide Hybrid Ligand Conjugation

Gurunath Apte[1,2] | Moritz Roman Schepp[1,2] | Haydn L. Ball[3,4] | Niklas Halbwedl[5] | Peijian Zou[6,7] | Na Sun[8] | Axel Walch[8] | Martin Zacharias[5] | Michael Sattler[6,7] | Oliver Plettenburg[3,4] | Jian Cui[1,2,9]

[1]Helmholtz Pioneer Campus, Helmholtz Munich, Neuherberg, Germany | [2]Photonic Biosystems and Technologies, Bioengineering Center, Helmholtz Munich, Neuherberg, Germany | [3]Institute of Medicinal Chemistry, Molecular Targets and Therapeutics Center, Helmholtz Munich, Neuherberg, Germany | [4]Institute of Organic Chemistry, Leibniz University Hannover, Hannover, Germany | [5]Department of Bioscience, TUM School of Natural Sciences, Physics Department and Center of Protein Assemblies, Technical University of Munich, Garching, Germany | [6]Institute of Structural Biology, Molecular Targets and Therapeutics Center, Helmholtz Munich, Neuherberg, Germany | [7]Bavarian NMR Center, Department of Bioscience, TUM School of Natural Sciences, Technical University of Munich, Garching, Germany | [8]Research Unit Analytical Pathology, Helmholtz Munich, Neuherberg, Germany | [9]Department of Bioscience, TUM School of Natural Sciences, Technical University of Munich, Garching, Germany

Correspondence: Jian Cui (jian.cui@helmholtz-munich.de)

Received: 1 June 2026 | **Revised:** 2 September 2026 | **Accepted:** 5 September 2026

Keywords: binding constant and kinetics | bio-orthogonal conjugation | complex biological media | hybrid peptides | optical biosensing | plasmonic nanoparticles | protein-protein interactions | surface functionalization

ABSTRACT

Protein–protein interactions (PPIs) govern most biological processes and are frequently altered in disease. However, in vitro characterization methods are often limited to binding affinities, specialized instrumentation, or are susceptible to extended-surface artifacts. Moreover, many remain incompatible with physiological media. Nano-optical biosensing based on nanoparticle (NP) localized surface plasmon resonances (LSPRs) offers an attractive in-solution alternative, but their performance has been limited in complex environments. Here, we present a solution-phase optical platform based on plasmonic nanoparticles functionalized with programmable peptide-hybrid ligands. We use sequence-defined ligands that combine nanoparticle anchoring, suppression of non-specific interactions, and site-specific bioconjugation. Unlike conventional polymers, these ligands are molecularly precise via solid-phase peptide synthesis. We show how this architecture effectively suppresses nonspecific adsorption while preserving colloidal stability and optical performance, and can be adapted to diverse protein targets through click chemistry and Sortase-mediated ligation. This platform enables high-sensitivity, label-free PPI detection via standard UV–vis spectrophotometry and minimal sample amounts. We quantify binding affinities of low molecular-weight proteins directly in undiluted serum, along with kinetic profiling in buffer. Furthermore, we demonstrate applicability over multiple protein pairs in buffer and serum, as well as proof-of-concept detection and quantification in human serum, highlighting its potential for future diagnostic applications.

1 | Introduction

Protein–protein interactions (PPIs) are central to the organization and regulation of biological systems, as most cellular functions are not carried out by individual proteins acting alone but by protein interactions with other biomolecules. These interactions control a variety of processes such as signal transduction, gene regulation, enzymatic activity, immune

Gurunath Apte and Moritz Roman Schepp contributed equally to this work. Each reserves the right to place their name first when citing this study in their curriculum vitae or elsewhere.

This is an open access article under the terms of the Creative Commons Attribution License, which permits use, distribution and reproduction in any medium, provided the original work is properly cited.
© 2026 The Author(s). *Small* published by Wiley-VCH GmbH

recognition, and structural organization within cells [1]. Disruptions to protein-protein interactions are associated with numerous diseases, including cancer, neurodegenerative disorders, and infectious diseases, making PPIs important targets for therapeutic intervention [2].

Quantitative measurements of protein-protein interaction parameters—particularly binding affinity, specificity, and kinetics—provide important mechanistic insights and can guide the development of therapeutics such as small molecules that compete with PPIs [3]. However, biologically relevant PPIs occur in complex biological environments. As such, development of PPI sensors that are compatible with complex biological fluids such as serum, cell lysate, or whole blood is critical for translating PPI measurements toward clinical and biomedical applications [4, 5]. There is a need for simple, reliable, and cost-efficient methods for detecting and quantifying PPIs in complex biological media for both fundamental research and biomedical applications.

Surface Plasmon Resonance (SPR) has long been considered the industry standard for the label-free measurement of protein binding affinities and kinetics [6]. However, traditional SPR platforms face several practical hurdles, including high instrumentation costs, a dependency on specialized microfluidics that can be prone to clogging from serum proteins [7], and the requirement for expensive metallic sensor chips with limited reuse [8]. Additionally, the presence of an extended planar surface can perturb the natural 3D diffusion of molecules, potentially interfering with the accuracy of binding measurements [9, 10].

Other common analytical techniques such as isothermal calorimetry (ITC), microscale thermophoresis (MST), and fluorescence anisotropy are limited to measuring equilibrium affinities, have limited sensitivity, have strict sample requirements, or are incompatible with complex biological media [11, 12]. Nuclear magnetic resonance (NMR) can provide unique insights into binding mechanisms, kinetics, and structure with residue-level resolution [13], but requires specific sample preparation and costly high-field instrumentation. Biolayer interferometry (BLI) and grating-coupled interferometry (GCI), which share conceptual similarities to SPR, are still dependent on costly instrumentation and extended planar surfaces [10, 14].

As a more accessible and cost-efficient alternative, in-solution localized surface plasmon resonance (LSPR) biosensors have been developed [15, 16]. This sensing principle employs noble-metal nanoparticles (NPs) whose LSPR confines and enhances electromagnetic fields within nanoscale near-field sensing volumes that enable highly localized molecular detection [17]. When biomolecules enter these volumes, they induce a change in the local refractive index, resulting in a shift in the LSPR extinction spectrum (Figure 1a) [18]. With highly sensitive silver-gold core-shell decahedral nanoparticles, interactions between proteins of <15 kDa molecular weight can be detected [16].

A key practical advantage of this approach is that these spectral shifts can be detected photometrically using standard UV–vis spectrophotometers, which are available in most laboratories, while also maintaining low material demands due to the minimal quantities of reagents and sample required for nanoparticle synthesis, functionalization, and measurement. Furthermore, with nanoparticle sensors diffusing freely in solution, artifacts originating from extended 2D surfaces are mostly avoided.

However, maintaining binding selectivity and sensitivity within physiological fluids remains a major challenge due to nanoparticle surface biofouling [19]. In such environments, high-abundance proteins and other biomolecules often adsorb onto NPs, forming a "biomolecular corona" that can mask the target signal [20]. Despite recent advances, existing approaches remain limited for quantitative, label-free PPI analysis in serum without the use of extended surfaces.

In our previous work, protein immobilization to nanobiosensors relied on poly-histidine tag ("His tag") coordination to Ni/NTA groups functionalized to nanoparticle surfaces [16]. While convenient, modular, and effective in buffer, this approach performs poorly in complex biological media such as serum. To enable nano-optical PPI sensing in such environments, two key challenges must be addressed: (1) minimizing nonspecific interactions with serum proteins and (2) maintaining specific interactions to proteins of interest (POI) and their binding partners.

Here, we introduce a strategy that borrows not from the antifouling literature, where polyethylene glycol (PEG), polyzwitterions, and poly(oxazoline)s are common [21], but from peptide synthesis. 2-[2-(2-Aminoethoxy)ethoxy]acetic acid (AEEA) is a short PEG-like building block commonly used in therapeutic peptides, like the side chain of tirzepatide [22], or with peptide nucleic acids (PNAs) as a flexible, soluble, and biocompatible linker [23, 24]. We employ it here as a nanoparticle surface ligand for antifouling, with anchoring to the nanoparticle gold surface achieved via cysteine-terminated thiol linkage [25, 26]. While all-peptide zwitterionic ligands can offer effective shielding, their reliance on canonical amino acids can also inadvertently introduce native peptide–protein recognition motifs. Our hybrid design avoids this by utilizing a poly(AEEA) spacer as the primary shielding layer, effectively eliminating amino-acid-based recognition sequences within the stealth domain while confining peptide blocks strictly to the anchoring and terminal targeting sites.

Because Cys-Poly(AEEA) is synthesized entirely via solid-phase peptide synthesis (SPPS), it is monodisperse and sequence-defined (Figure S1), avoiding the polydispersity inherent in conventional polymer-based ligands. This architecture integrates three required functions—surface anchoring, antifouling, and distal bioconjugation handles—within a single ligand sequence. In principle, the use of precise sequence-defined surface ligands promotes batch-to-batch reproducibility and quantitative interpretation of binding assays, as each ligand is molecularly defined. Moreover, poly(AEEA) length, linker spacing, and bioconjugation motifs (SPAAC-compatible azide, Sortase recognition sequence, etc.) [27, 28] can be independently optimized through iterative SPPS design—an advantage more easily achieved compared to most polymer variants.

We have developed and validated a highly specific in-solution nanoparticle-based LSPR platform with sequence-defined hybrid peptide ligands for anti-fouling and site-specific, bio-orthogonal

16136829, 0, Downloaded from https://onlinelibrary.wiley.com/doi/10.1002/smll.75794, Wiley Online Library on [09/11/2026]. See the Terms and Conditions (https://onlinelibrary.wiley.com/terms-and-conditions) on Wiley Online Library for rules of use; OA articles are governed by the applicable Creative Commons License

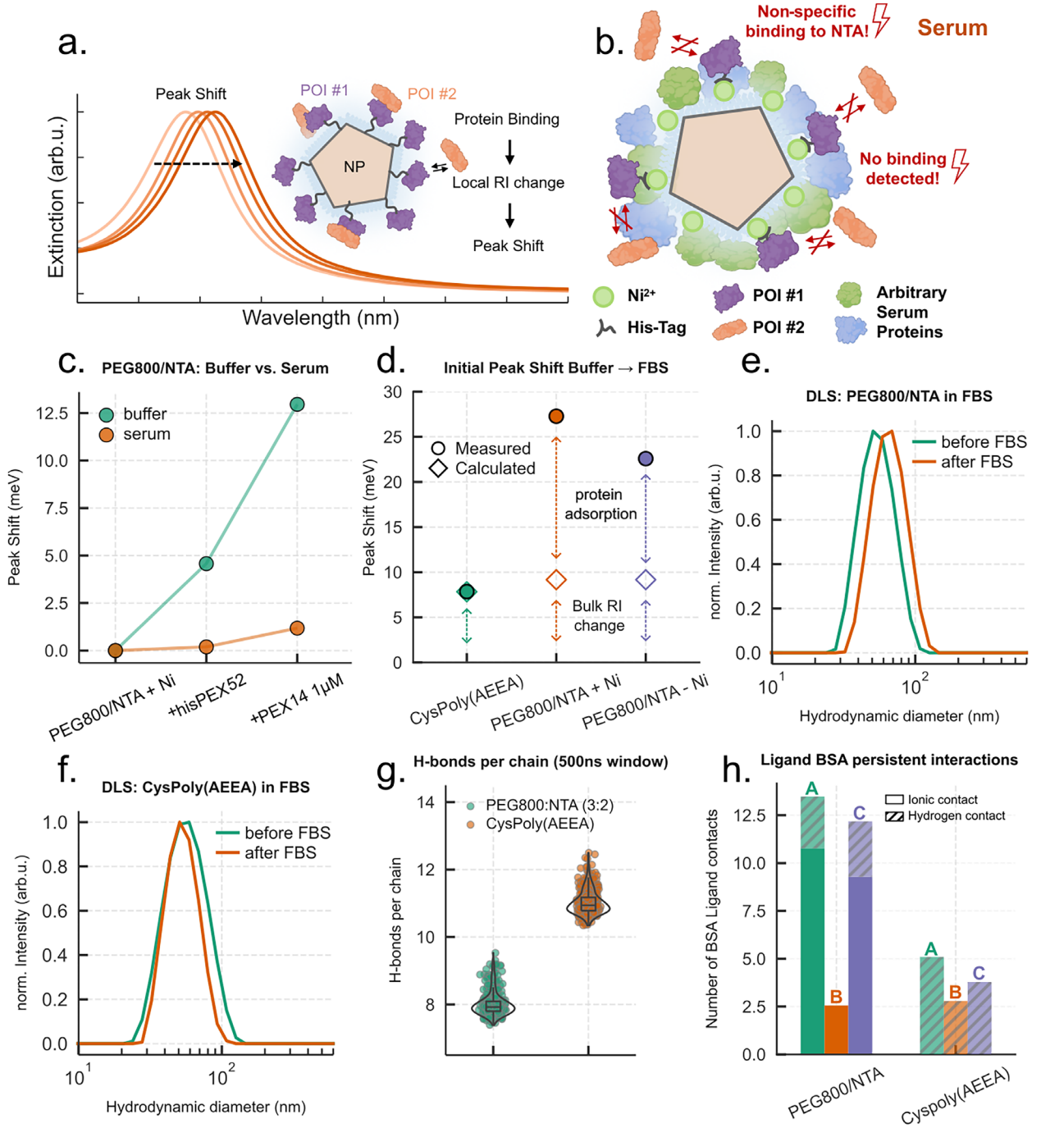


FIGURE 1 | Antifouling Hybrid Peptide Ligands for Protein-Protein Interaction Sensing. (a) Schematic of the solution-phase nanobiosensor operating principle for detecting protein–protein interactions. Target protein (POI2) binding to proteins of interest (POI1) on the nanoparticle surface increases the local refractive index, causing red-shifts of the LSPR peak. The magnitude of the shift scales with the surface coverage of bound protein. (b) Cartoon illustrating the challenge of solution-based LSPR biosensing in complex media using nanobiosensors with the Ni/NTA bioconjugation strategy. In a complex biological medium, such as fetal bovine serum (FBS), nonspecific interactions and protein corona formation lead to diminished sensor capability. (c) Scatterplot showing the cumulative LSPR spectral shifts of modified nanosensors in buffer and undiluted FBS. Upon addition of His-PEX52 (15 nM) followed by its interaction partner PEX14 (1 μM for full binding saturation), no apparent LSPR shift was observed in FBS, whereas clear LSPR shifts corresponding to protein binding were observed in buffer (Table S2). (d) Comparison of measured and calculated LSPR peak shifts upon transfer from buffer to FBS for NPs functionalized with PEG800:NTA ($\pm Ni^{2+}$) and CysPoly(AEEA) hybrid ligands (Table S1). Hydrodynamic diameter distributions of (e) PEG800:NTA and (f) CysPoly(AEEA)-functionalized NPs measured by dynamic light scattering (DLS) before and after incubation in FBS. (g) Violin plots with data points showing the number of hydrogen bonds with surrounding water molecules per average surface brush for Cys–Poly(AEEA)-modified and thiol-PEG800:NTA–Ni^{2+}-modified gold surfaces over a 500 ns MD simulation (Figure S6). (h) Cumulative number of BSA residues forming specific and persistent contacts (i.e., contacts present after 100 ns), including ionic interactions (salt bridges and Ni^{2+} coordination) and hydrogen bonds (Figure S5), with surface brushes of mixed thiol-PEG800:NTA–Ni^{2+} or Cys–Poly(AEEA) modified gold surfaces, for three BSA orientations (Figure S7), A (teal), B (orange), and C (purple), over a 1000 ns MD simulation.

16136829, 0, Downloaded from https://onlinelibrary.wiley.com/doi/10.1002/smll.75794, Wiley Online Library on [09/11/2026]. See the Terms and Conditions (https://onlinelibrary.wiley.com/terms-and-conditions) on Wiley Online Library for rules of use; OA articles are governed by the applicable Creative Commons License

protein immobilization. This system enables reliable and quantitative determination of thermodynamic and kinetic binding parameters in both buffer and undiluted animal serum via standard UV–vis spectrophotometry. We demonstrate specific detection of multiple protein–protein interactions, including intrinsically disordered protein regions or small proteins (<15 kDa), and quantification of target analytes at defined concentrations directly in human serum — addressing a critical unmet need in bioanalytical PPI sensing and highlighting the platform's clinical and diagnostic potential.

2 | Results and Discussion

To establish a solution-phase nanoparticle biosensing platform for PPI detection, we previously developed high-sensitivity Au-coated Ag decahedral nanoparticles (AgDNP@Au) functionalized with PEG:NTA ligands for immobilization of polyhistidine-tagged proteins of interest (POI-1) through Ni^{2+} coordination (Figure 1b). The NPs were synthesized using a home-built photoreactor, with an updated model shown in Figure S2, and unfunctionalized AgDNP@Au characterized using electron microscopy and dynamic light scattering (Figure S3). This assembly allowed efficient and convenient detection of binding thermodynamics and kinetics between POI-1 and its partner, POI-2, in buffer [16].

However, the performance of these nanobiosensors has been significantly compromised in complex biological media such as fetal bovine serum (FBS, Figure 1b). Figure 1c directly compares the PPI sensing performance of PEG800:NTA-functionalized nanobiosensors in buffer versus serum, using the interaction between two peroxisomal proteins as a well-characterized model system: the intrinsically disordered N-terminal domain of Peroxisomal Biogenesis Factor 5 ("PEX5") and the globular N-terminal domain of Peroxisomal Biogenesis Factor 14 ("PEX14"). Two PEX5 constructs were employed — "PEX51" (residues 1–113, Table S4) and "PEX52" (residues 110–230, Table S4) — alongside "PEX14" (residues 16–80, Table S4) [16, 29].

In buffer, sequential addition of His-PEX52 (POI-1) to nanobiosensors, followed by its interaction partner PEX14 (POI-2), produced subsequent LSPR peak shifts, confirming successful protein immobilization and protein-protein binding, and thus validating sensor functionality (Figure 1c). In contrast, no LSPR shifts indicative of specific protein binding were detected in serum. Critically, even pre-functionalization of the nanosensor surface with His-PEX5 failed to restore sensing capability, as no LSPR shift was observed upon subsequent PEX14 addition (Figure S4).

To further pinpoint the origin of this effect, we compared the initial LSPR peak shift upon nanoparticle exposure to serum with the shift expected solely from the bulk refractive-index (RI) difference between water and FBS ($\Delta RI = 0.0099$), as determined by refractometry. For CysPoly(AEEA)-functionalized NPs, the measured initial LSPR shifts closely matched the calculated bulk refractive index change (Figure 1d), indicating negligible contributions from extensive protein adsorption at nanoparticle surfaces. In contrast, PEG800:NTA-functionalized NPs both with and without Ni^{2+} exhibited substantially larger shifts than predicted from bulk refractive index alone. We attribute this additional shift to non-specific adsorption of serum proteins onto the nanosensor surface.

This interpretation is further supported by dynamic light scattering (DLS) measurements of hydrodynamic diameter after incubation in undiluted FBS and subsequent washing. The washing step selectively removes loosely adsorbed proteins of the "soft" corona while retaining the tightly bound "hard" corona [19, 30]. PEG800:NTA-coated AgDNP@Au exhibited an increase in hydrodynamic diameter of ~15 nm (Figure 1e), consistent with substantial serum protein adsorption [31] and the formation of a stable hard protein corona [32]. In contrast, NPs functionalized with CysPoly(AEEA) hybrid ligands showed a negligible size decrease of ~5 nm after washing (Figure 1f), indicating that no hard corona was retained under identical conditions. The absence of a measurable hard corona suggests that CysPoly(AEEA) hybrid ligands either prevent strong nonspecific protein adsorption altogether or promote the formation of a soft, dynamic corona that is readily displaced upon washing [33, 34]. A dynamic, soft corona would present a lower steric and energetic barrier to analyte access, facilitating specific binding at the sensor surface in complex biological media.

To explore the mechanistic basis for the contrasting antifouling behavior of the two ligand systems, we performed atomistic molecular dynamics (MD) simulations for PEG800:NTA (3:2) and CysPoly(AEEA) ligands grafted to a gold surface via thiol linkages (Figure S6) and examined two key properties. First, we assessed brush hydration over a 500 ns simulation window, as the capacity of polymer brushes to retain water molecules is a well-established indicator of antifouling performance (Figure 1g and Figure S6 for time traces) [35]. According to these calculations, we found that PEG800:NTA brushes formed a median of 8 hydrogen bonds per chain with surrounding water molecules, compared to 11 for CysPoly(AEEA) brushes. The substantially higher hydration of the CysPoly(AEEA) system implies that a greater number of water molecules must be displaced prior to non-specific protein adsorption, providing one molecular-level explanation for its superior antifouling properties relative to ' PEG800:NTA.

Second, to evaluate direct ligand–protein interactions, we quantified persistent contacts between the ligands and BSA (i.e., sustained for >100 ns) over a 1000 ns simulation across three distinct BSA orientations relative to the surface (denoted A, B, and C in Figure 1h and Figure S7). Here, we selected BSA for modeling as it is the most abundant protein found in serum and, subsequently, on nanoparticle surfaces upon insufficient surface passivation [36]. For PEG800:NTA, the charged character of the NTA ligand drove predominantly ionic interactions across all three orientations, manifesting as salt bridges between NTA carboxylate groups and basic BSA residues (Lys/Arg), coordinate bonds between surface-chelated Ni^{2+} and acidic residues (Asp/Glu), with additional hydrogen bond contacts in orientations A and C. In contrast, CysPoly(AEEA) ligands exhibited markedly fewer persistent contacts across all BSA orientations, which were exclusively hydrogen bond-mediated, with no ionic interactions, as the CysPoly(AEEA) ligands are uncharged. This distinction has direct thermodynamic consequences: Ni^{2+} coordination bonds and salt bridges generally exceed the strength of hydrogen bonds

16136829, 0, Downloaded from https://onlinelibrary.wiley.com/doi/10.1002/smll.75794, Wiley Online Library on [09/11/2026]. See the Terms and Conditions (https://onlinelibrary.wiley.com/terms-and-conditions) on Wiley Online Library for rules of use; OA articles are governed by the applicable Creative Commons License

[37–39], making BSA substantially more prone to non-specific adsorption onto PEG800:NTA than onto CysPoly(AEEA), where only weaker, more transient contacts persist.

To isolate the contribution of the ligand scaffold itself from that of NTA/Ni^{2+}, we compared CysPoly(AEEA) against molecular-weight-matched, NTA-free PEG thiols on the same nanoparticle batch. We found that CysPoly(AEEA) maintained colloidal stability where SH-PEG800 induced aggregation, and that CysPoly(AEEA)-N_3 gave a narrower LSPR linewidth than SH-PEG-N_3 (237 vs. 306 meV), corresponding to a ~23% higher figure of merit, assuming equal refractive-index sensitivity (Figure S8).

Altogether, these experiments and simulations support a model of nonspecific adsorption of serum proteins to the nanoparticle surface leading to the formation of a "hard", relatively impermeable protein corona, perhaps via interactions with charged groups such as NTA. This corona can sterically and electrostatically hinder the accessibility of NP surface binding sites both for His-POI-1 immobilization and subsequent binding of POI-2.

Overall, our results demonstrate that CysPoly(AEEA) hybrid ligands confer superior antifouling properties relative to the previous PEG/NTA system, serving as a foundation for reliable biosensing performance in complex biological environments.

Having established the antifouling properties of CysPoly(AEEA), we next introduced site-specific bioconjugation for protein immobilization to the nanosensor surface. As our simulations implicate ionic contacts as key drivers of nonspecific binding in the PEG:NTA system (Figure 1g,h), we designed two uncharged CysPoly(AEEA) variants with distinct terminal functional groups (Table S1 and Figure S9), each enabling site-specific covalent protein attachment in place of the non-covalent Ni^{2+}-His-tag approach (Figure 2a).

For the first strategy, we used strain-promoted azide–alkyne cycloaddition (SPAAC) click chemistry. First, we engineered a C-terminal cysteine residue to our POI-1 and reacted the cysteine thiol with a maleimide–dibenzocyclooctyne (DBCO) linker, generating a protein–DBCO conjugate [40]. Successful conjugation and a degree of labeling of 0.79 were confirmed by UV–vis spectroscopy from extinction at 280 and 309 nm (Figure S10). Next, we reacted the DBCO-functionalized protein with an organic azide (azido-alanine) positioned at the C-terminus of the CysPoly(AEEA) hybrid ligand (Table S1) via 1,3-dipolar cycloaddition, producing a highly stable covalent 1,2,3-triazole linkage [41].

In the second bioconjugation strategy, we used Sortase-A mediated ligation to achieve site-specific covalent immobilization of POI-1. We synthesized a CysPoly(AEEA) hybrid ligand functionalized with a C-terminal Sortase recognition motif (LPETGGG, Table S1 and Figure S9) [42]. Upon addition of the mutant Sortase4M [43], the enzyme catalyzes a two-step transpeptidation reaction. First, cleavage occurs between the threonine and glycine residues of the LPETGGG motif via nucleophilic attack by the active-site cysteine of Sortase4M, forming a thioacyl intermediate. In the second step, an N-terminal glycine-modified ligand protein resolves this intermediate, resulting in covalent ligation of the protein to the CysPoly(AEEA) ligand. The requirement for an N-terminal glycine as the nucleophile, as well as the optimal ligation time, was confirmed using a bacterial Sortase substrate assay, which showed that ligation proceeds selectively with glycine-modified proteins and not with proteins bearing alternative N-terminal residues (Figure S11). Successful ligation was confirmed by MALDI-TOF mass spectrometry (Figure S12). Further optimization revealed that a 10:1:10 molar ratio (ligand:Sortase:protein) yielded the most efficient conjugation, as evidenced by MALDI-TOF analysis (Figure S13).

Notably, for both bioconjugation strategies, nanobiosensor assembly required pre-ligation of protein to the CysPoly(AEEA) ligand in solution prior to nanoparticle grafting, as direct conjugation to ligand-functionalized NPs was ineffective (data not shown). This is consistent with reports that steric hindrance at crowded surfaces limits reactive terminus accessibility for both SPAAC and SML [44, 45]. Hence, we first formed the pre-conjugate, which was then grafted onto the NP surface for both SPAAC and SML.

In the final step of nanobiosensor assembly, we performed backfilling using shorter CysPoly(AEEA) ligands [46]. By filling unfunctionalized gaps of the sensor surface, this treatment substantially enhanced the stability and antifouling properties of the nanobiosensors. The detailed workflow for peptide–protein conjugation followed by nanoparticle immobilization to generate the nanobiosensors is illustrated schematically in Figure S14. This process includes the removal of unreacted His-tagged Sortase using magnetic Ni-NTA beads, as demonstrated in Figure S15.

To quantify the surface functionalization, supernatant depletion assays yielded a Cys-poly(AEEA) grafting density of 2.2 ligands/nm^2 (Figure S16) and a protein surface coverage of 0.14 proteins/nm^2 (PEX52C, Figure S17, Supplementary Discussion).

Successful conjugation was further confirmed spectroscopically: Figure 2b,c displays the UV–vis spectra of unfunctionalized NPs, NPs functionalized with CysPoly(AEEA) ligands alone, and NPs conjugated to proteins via SPAAC and SML, respectively. Upon functionalization, a red shift of the plasmon resonance peak was observed relative to the unfunctionalized NPs. Furthermore, for both conjugation strategies, functionalization was accompanied by an increase in hydrodynamic diameter and ζ-potential relative to the as-synthesized and ligand-only NP controls (Figure 2d,e). The measured ζ-potential values following protein conjugation remain within ranges commonly reported for stable colloidal NP dispersions [47].

To further characterize the platform, we benchmarked sensing performance using the well-characterized, high-affinity biotin–streptavidin interaction, measuring streptavidin binding to biotin-functionalized nanobiosensors conjugated via SPAAC (Figure 2f and Figure S18). From a fit to the linear range of the concentration curve and the standard deviation of repeated peak measurements (Figure 2f and Figure S18c), we measured a limit of detection (LOD) of 43 pM. Notably, no LSPR shifts were detected for nanosensors functionalized with CysPoly(AEEA) without biotin (Figure 2f). The determined LOD for biotin-streptavidin is competitive with chip- and fiber-based LSPR sensors reporting values in the low-picomolar range (2 pM, 94 pM) [48, 49], and notably outperforms other colloidal solution-phase systems,

16136829, 0, Downloaded from https://onlinelibrary.wiley.com/doi/10.1002/smll.75794, Wiley Online Library on [09/11/2026]. See the Terms and Conditions (https://onlinelibrary.wiley.com/terms-and-conditions) on Wiley Online Library for rules of use; OA articles are governed by the applicable Creative Commons License

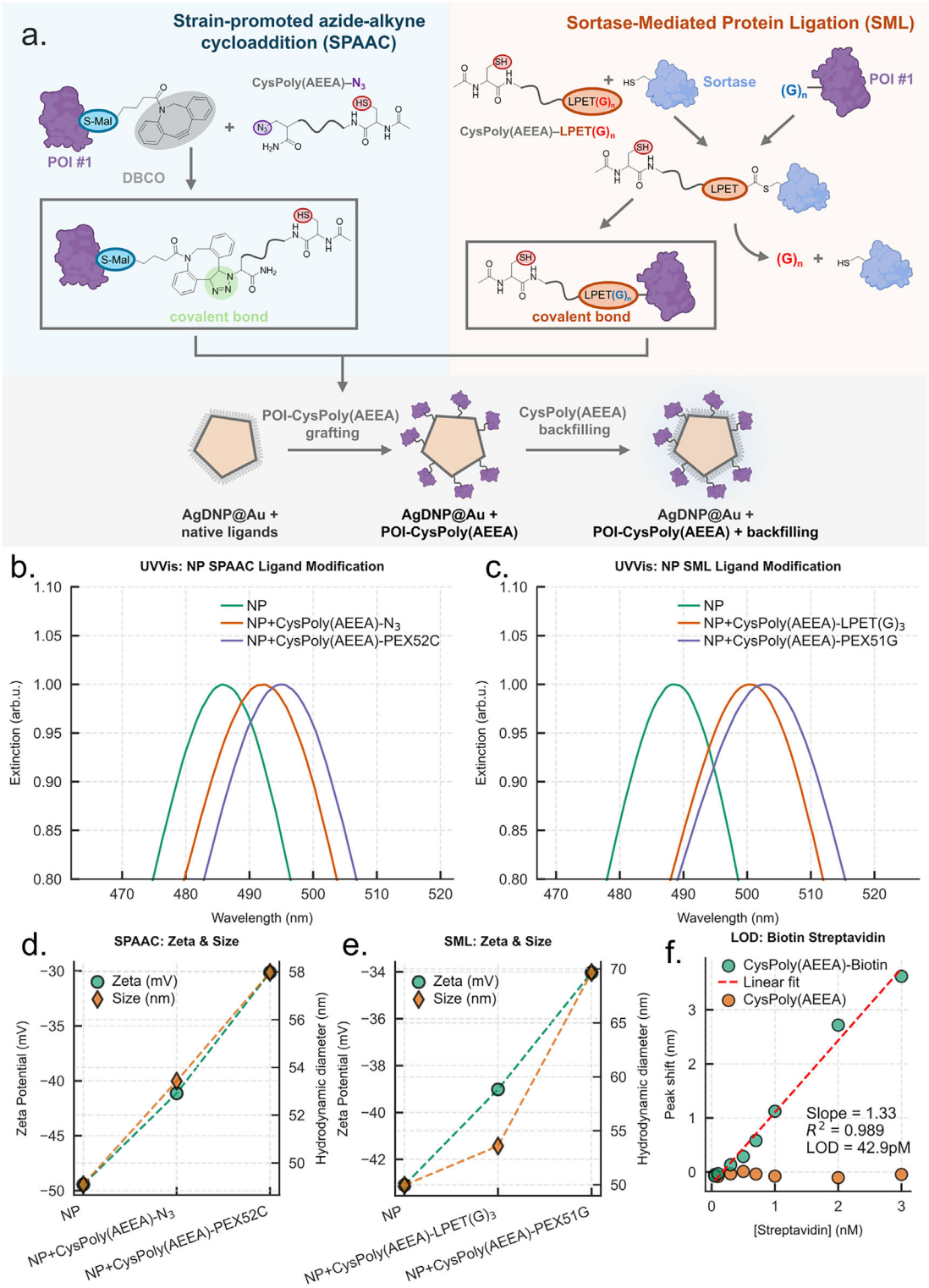


FIGURE 2 | Modular Covalent Protein Attachment to Nanosensors via CysPoly(AEEA) Ligands (a) Schematic of two strategies for covalent bioconjugation of a protein of interest (POI) to the CysPoly(AEEA) hybrid ligand: strain-promoted azide–alkyne cycloaddition (SPAAC, left) and Sortase-mediated ligation (SML, right). Bottom, grey box: illustration of surface chemistries and intermediate steps in modification of NPs for both methods. (b,c) Cropped extinction spectra of nanosensors during stepwise surface functionalization via (b) SPAAC and (c) SML. Teal: unfunctionalized nanoparticles (LSPR); orange: CysPoly(AEEA) ligands; purple: final nanobiosensor with CysPoly(AEEA)–POI, where PEX52 (SPAAC) and PEX51 (SML) were bioconjugated (Tables S1 and S4). (d,e) Scatter plots showing changes in zeta potential and hydrodynamic diameter of nanosensors at each functionalization step: unfunctionalized, after CysPoly(AEEA) grafting, and after CysPoly(AEEA)–POI conjugation via (d) SPAAC and (e) SML. Note that different NP batches were used for the respective experiments. (f) Binding titration curve for biotin-conjugated nanobiosensors via SPAAC, showing the response to streptavidin addition within the linear range. CysPoly(AEEA) functionalized NPs without biotin were used as a control. The limit of detection (LOD) was calculated by dividing 3 times the LSPR peak deviation (Figure S18c) by the sensitivity (slope of the linear fit).

16136829, 0, Downloaded from https://onlinelibrary.wiley.com/doi/10.1002/smll.75794, Wiley Online Library on [09/11/2026]. See the Terms and Conditions (https://onlinelibrary.wiley.com/terms-and-conditions) on Wiley Online Library for rules of use; OA articles are governed by the applicable Creative Commons License

which have only reached low-nanomolar (5 nM, 3 nM) sensitivity [50, 51]. These results demonstrate that covalent poly(AEEA) functionalization maintains high sensing performance, while enabling operation in complex biological media (Figure S18).

We quantified protein-protein interactions using CysPoly(AEEA)-functionalized NP biosensors for both bioorthogonal conjugation approaches. For the PEX52–PEX14 interaction pair, NP biosensors were functionalized with CysPoly(AEEA) hybrid ligands using SPAAC chemistry. PEX52 was site-specifically labeled via maleimide–DBCO conjugation and reacted with CysPoly(AEEA)-azide before grafting onto the NP surface.

For PEX5 protein constructs, conjugation handles were introduced at the C-terminus of each construct for both SML (glycine) and SPAAC (cysteine) to minimize perturbation of the native binding interface [52].

Titration with PEX14 produced a binding curve that fit the Hill–Waud equation, giving an apparent K_D of 350 ± 51 nM (Figure 3a). Control experiments with BSA as POI-2 or without immobilized PEX52 showed no detectable binding. In the case of the PEX51–PEX14 binding pair, PEX51 was immobilized on the NP surface via SML. Titration with PEX14 constructs yielded a saturable, concentration-dependent response, also fitted with the Hill–Waud equation, resulting in a K_D of 330 ± 39 nM (Figure 3b). Binding was again absent in controls using BSA or in the absence of immobilized PEX51, confirming interaction specificity.

The apparent dissociation constants measured here for the PEX51–PEX14 interaction are in close agreement with values reported in our previous work ($K_D \approx 289$ nM) [16] and are consistent with measurements obtained using isothermal titration calorimetry (~157 nM) [53] and surface plasmon resonance (~87 nM) [52]. Similarly, the PEX52–PEX14 affinities measured using SPAAC-functionalized biosensors are consistent with prior reports ($K_D \approx 171$ nM) and fall within the range determined by isothermal titration calorimetry (~139–344 nM) [53]. Together, these results establish that both SPAAC and SML functionalization strategies support robust and reliable quantification of equilibrium binding affinities consistent with other established biophysical measurement techniques.

Quantifying biomolecular interactions consists of more than equilibrium dissociation constants – kinetic information is valuable and an important consideration in drug discovery [54]. We used our CysPoly(AEEA)-functionalized NP biosensors for measuring real-time kinetics of both PEX51–PEX14 and PEX52–PEX14 binding (Figure 3c,d). To achieve sufficient temporal resolution, measurements were conducted by monitoring the LSPR extinction at a single wavelength positioned at the point of maximum absolute slope on the red side of the LSPR spectrum (Figure S19). To ensure sufficient signal-to-noise ratio, POI-2 was added at concentrations above the apparent K_D ($\approx 3 \times K_D$,). Representative kinetic traces for PEX52–PEX14 and PEX51–PEX14 were fitted with a single exponential function, yielding observed rate constants of $k_{obs} = 0.141 \pm 0.004$ s^{-1} and $k_{obs} = 0.231 \pm 0.009$ s^{-1}, respectively. Combined with the equilibrium dissociation constants determined above, association and dissociation rate constants were calculated to be $k_a = (1.04 \pm 0.05) \times 10^5$ $M^{-1}s^{-1}$, $k_d = (3.7 \pm 0.4) \times 10^{-2}$ s^{-1} for PEX52–PEX14, and $k_a = (1.7 \pm 0.1) \times 10^5$ $M^{-1}s^{-1}$, $k_d = (5.7 \pm 0.6) \times 10^{-2}$ s^{-1} for PEX51–PEX14. These rates are in good agreement with previous reports [16, 52], with deviations possibly due to mass transport differences between different techniques.

To assess the modularity and broader applicability of our platform, we measured several additional low-molecular-weight protein-protein interaction pairs (6–14 kDa, Table S4), including TAD–NCBD, TAD–MDM2, and ACTR–NCBD, using both bioconjugation methods. In these measurements, POI-1 was immobilized onto CysPoly(AEEA)-functionalized NPs using either SPAAC or SML, followed by addition of the corresponding interaction partner POI-2 at concentrations near literature K_D values (Table S3) [55, 56]. For each protein pair, specificity was evaluated against parallel negative controls in which BSA was added instead of POI-2 at the same concentrations (Figure 3e,f). In all cases tested, the target binding partner produced a measurable spectral shift, whereas BSA controls showed negligible shifts, demonstrating that both immobilization strategies reliably support detection of diverse PPIs with high specificity and minimal nonspecific fouling in buffer.

Having established robust equilibrium and kinetic binding measurements in buffer using both immobilization strategies, we next evaluated the performance of our NP biosensors in complex biological media. Specifically, we quantified the equilibrium binding of the PEX52–PEX14 and PEX51–PEX14 interactions in undiluted fetal bovine serum (FBS). As in buffer-based experiments, appropriate control measurements (without POI-1, addition of BSA) were performed to assess nonspecific interactions. Prior to binding measurements, the nanobiosensors were incubated in FBS for 1 h to allow for equilibration of the NP surface. UV–vis spectra recorded before and after incubation and throughout the binding titration measurements showed no evidence of nanoparticle aggregation, as supported by the absence of peak broadening or shoulder formation (Figure S20).

Equilibrium binding isotherms obtained under these conditions yielded apparent dissociation constants K_D that were comparable to those measured in buffer (PEX52–PEX14: 350 nM in buffer vs. 470 nM in FBS; PEX51–PEX14: 330 nM vs. 320 nM), indicating that the serum environment did not substantially perturb binding affinity or sensor performance (Figure 4a,b). This is consistent with the negligible response to BSA addition to the PEX5-functionalized nanobiosensors in buffer (Figure 3a,b). Notably, unlike our previous NTA–Ni–His-tag protein immobilization strategy with impaired sensing in serum (Figure 1b), the functionalized peptide hybrid ligands used here provide an antifouling interface while permitting specific interactions. This preserves sensor functionality and enables reliable measurements in complex biological environments such as undiluted FBS.

The K_D values measured by our technique were broadly consistent with literature values, although deviations of ~2 to 4-fold were observed. Indeed, previous measurements of nearly identical PEX5 and PEX14 constructs using ITC and SPR resulted in up to 3.3-fold variations in K_D [53]. Such variations are common when comparing highly disparate biophysical techniques. Unlike ITC, which measures binding thermodynamics in solution without any modifications, our platform utilizes site-specific,

16136829, 0, Downloaded from https://onlinelibrary.wiley.com/doi/10.1002/smll.75794, Wiley Online Library on [09/11/2026]. See the Terms and Conditions (https://onlinelibrary.wiley.com/terms-and-conditions) on Wiley Online Library for rules of use; OA articles are governed by the applicable Creative Commons License

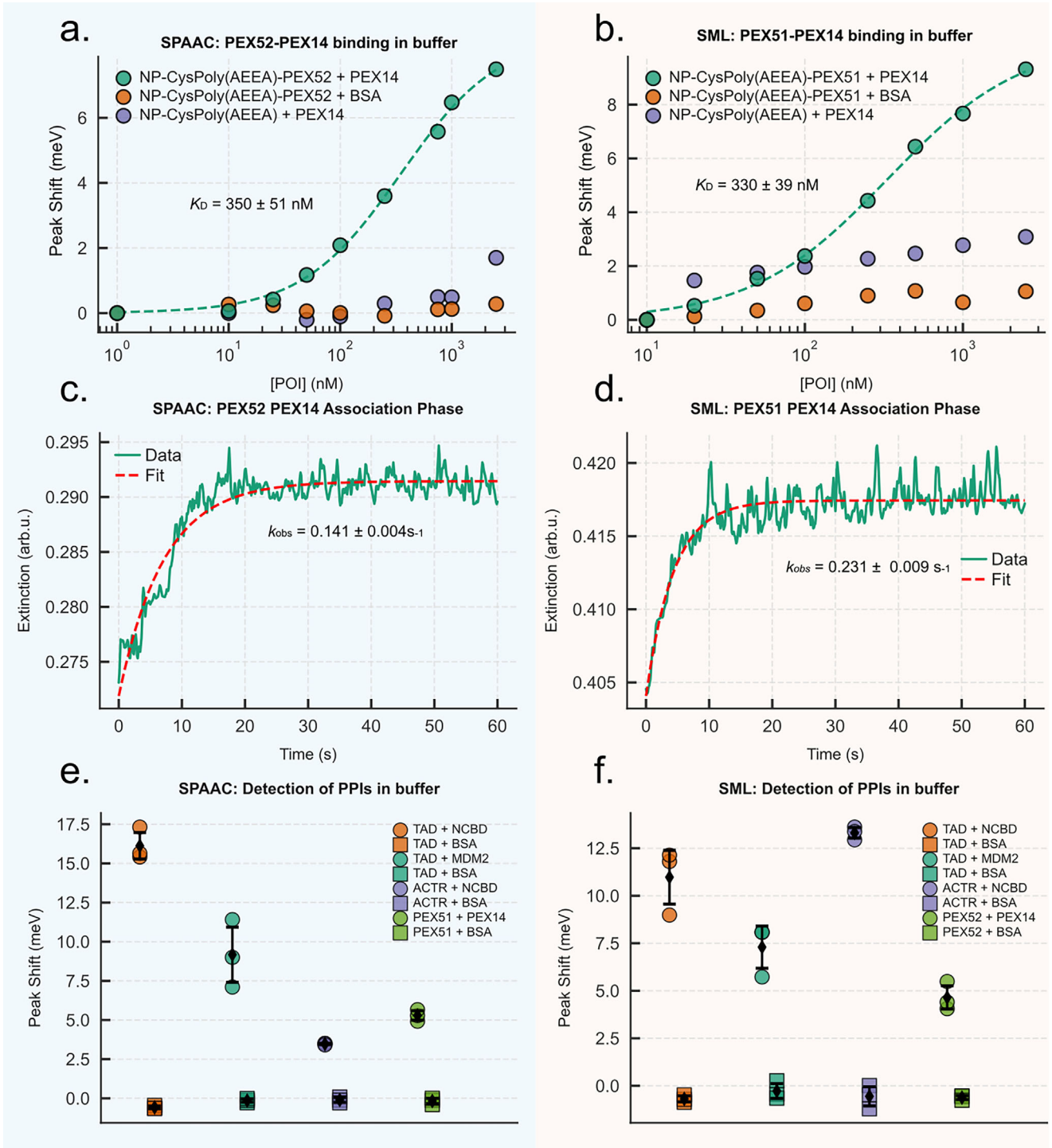


FIGURE 3 | PPI detection and quantification in buffer. (a,b) Equilibrium binding curves of PEX5–PEX14 interactions measured with nanobiosensors prepared via both bioconjugation strategies: (a) PEX52 via SPAAC and (b) PEX51 via SML. POIs were immobilized via the respective methods, and binding was assessed by LSPR peak shifts upon PEX14 titration. Data were fitted with the Hill–Waud equation to determine apparent K_D values; uncertainties represent one standard deviation from the least-squares covariance matrix. No binding was observed in controls using BSA addition or in the absence of immobilized protein. (c,d) Representative kinetic traces for PEX5–PEX14 binding at concentrations ~3×K_D for (c) SPAAC and (d) SML. Traces were fitted with a single exponential function to extract the observed rate constant (k_{obs}), with uncertainties representing one standard deviation from the least-squares covariance matrix. (e,f) LSPR peak shifts of nanobiosensors functionalized via (e) SPAAC or (f) SML with different protein-protein interaction partners (TAD–NCBD, TAD–MDM2, ACTR–NCBD, PEX5–PEX14). Target binding partners and BSA controls were added at concentrations near reported K_D values (Table S3). Markers with error bars indicate the mean ± one standard deviation of three measurements. For PEX5–PEX14, panels (e,f) show the complementary PEX5 construct to (a,b): PEX51 via SPAAC in (e), PEX52 via SML in (f), confirming that both constructs are compatible with either conjugation strategy.

16136829, 0, Downloaded from https://onlinelibrary.wiley.com/doi/10.1002/smll.75794, Wiley Online Library on [09/11/2026]. See the Terms and Conditions (https://onlinelibrary.wiley.com/terms-and-conditions) on Wiley Online Library for rules of use; OA articles are governed by the applicable Creative Commons License

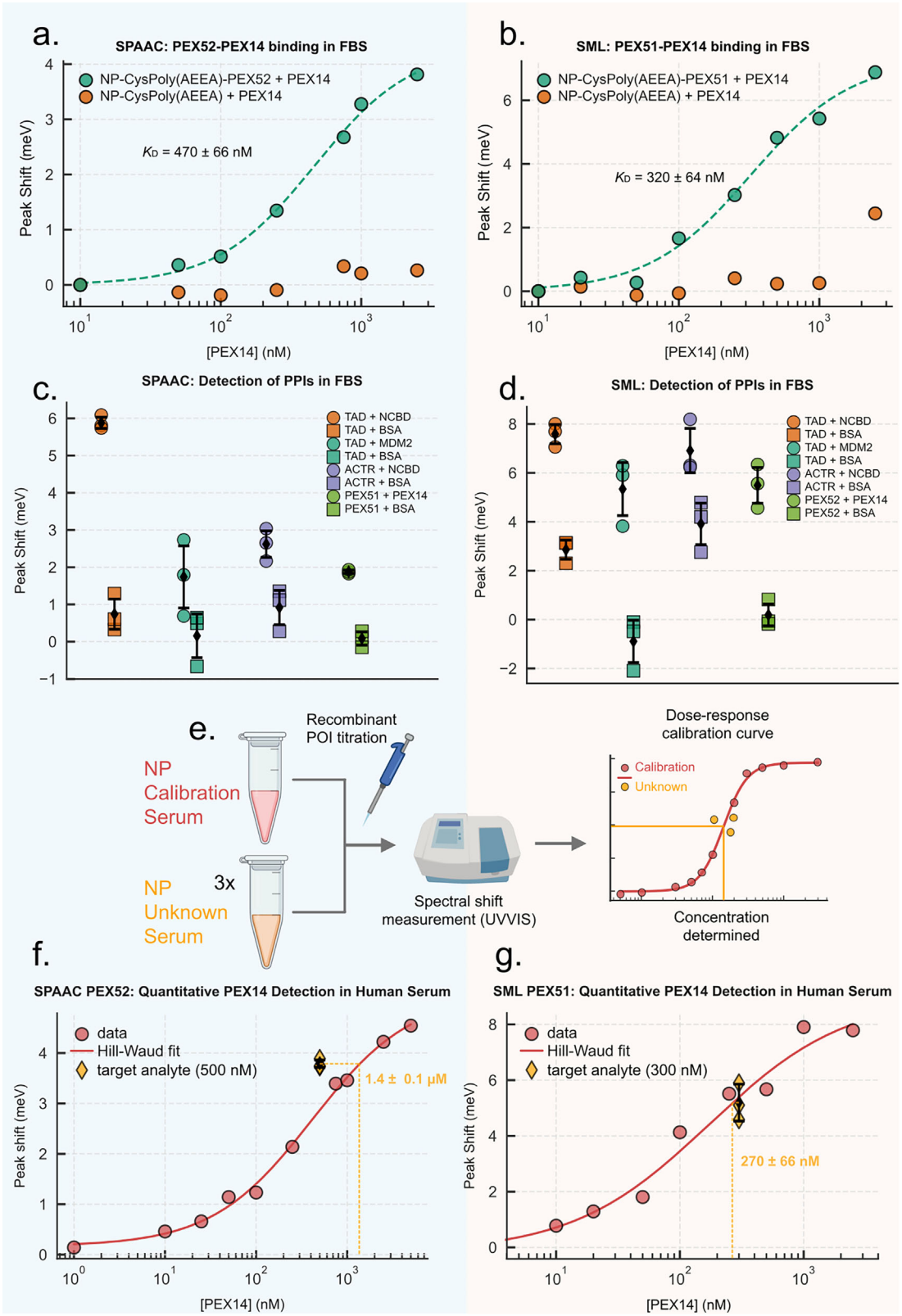


FIGURE 4 | PPI detection and quantification in serum. (a,b) Equilibrium binding curves obtained from LSPR peak shifts for PEX5–PEX14 interactions with proteins immobilized via (a) SPAAC (PEX52) or (b) SML (PEX51). Binding curves were fitted using the Hill–Waud equation to obtain K_D, with no binding observed in controls lacking immobilized protein. Uncertainties represent one standard deviation from the least-squares covariance matrix. (c,d) LSPR responses of nanobiosensors functionalized with different PPI binding pairs (TAD–NCBD, ACTR–NCBD, PEX5–PEX14 and TAD-MDM2 (Table S3)) via (c) SPAAC and (d) SML. Target-binding proteins and BSA controls were added at concentrations near reported K_D values (Table S3). Markers with error bars indicate the mean ± one standard deviation of three measurements. (e) Schematic of the diagnostic human serum workflow: POI-1–functionalized nanobiosensors were first calibrated (red) by titration with recombinant POI-2, then used to quantify POI-2 in an unknown serum

16136829, 0, Downloaded from https://onlinelibrary.wiley.com/doi/10.1002/smll.75794, Wiley Online Library on [09/11/2026]. See the Terms and Conditions (https://onlinelibrary.wiley.com/terms-and-conditions) on Wiley Online Library for rules of use; OA articles are governed by the applicable Creative Commons License

bio-orthogonal surface tethering. While this targeted immobilization prevents random orientation, covalent anchoring unavoidably restricts local degrees of freedom and steric accessibility, potentially affecting apparent binding. Furthermore, compared to traditional planar SPR channels, our in-solution nanoparticle configuration operates under different mass-transport regimes. Despite these different conditions, the reasonably close quantitative agreement demonstrates that the platform offers a simple, yet robust and quantitative characterization method even directly in complex media.

To further assess reproducibility, we performed additional PEX5–PEX14 binding measurements via both SPAAC and SML in buffer and FBS, conducted by different researchers on independent nanoparticle batches and on different days (Figure S21). The resulting K_D values (360 ± 56 nM SPAAC/buffer, 340 ± 45 nM SML/buffer, 240 ± 130 nM SPAAC/FBS, 320 ± 75 nM SML/FBS) fell within the same 2- to 4-fold range noted above, indicating that this spread reflects typical assay-to-assay variability rather than an artifact of a specific operator, nanoparticle batch, or conjugation chemistry.

We next examined several additional protein-protein interaction pairs in undiluted serum, as in Figure 3e,f in buffer (Table S3). We tested these interaction pairs (TAD–NCBD, TAD–MDM2, ACTR–NCBD, PEX51-PEX14, PEX52-PEX14) in undiluted FBS via both bioconjugation techniques (Figure 4c,d). Here, we measured distinct differences between the addition of the target binding partner relative to the BSA control. Although signal amplitudes were slightly reduced relative to buffer experiments (Figure 3e,f), specific PPI responses remained readily detectable, demonstrating robust sensor performance for a variety of protein pairs in complex biological media.

We note, however, that absolute peak-shift magnitudes are not directly comparable between the two conjugation strategies. The LSPR response depends not only on binding affinity but also on how the analyte is presented within the sensing volume, since the plasmonic near-field decays steeply with distance from the particle surface. Although both routes are site-specific and address the same terminus of POI1, they differ in linker architecture: SML through a Cys-$(AEEA)_5$-LPETGGG tether, SPAAC through a Cys-$(AEEA)_7$-N_3/DBCO-triazole adduct, which results in differences in spacer length, flexibility, and terminal group bulk that can shift the average height and orientational ensemble of the tethered protein. These linker-architecture effects are the likely origin of the differing peak-shift magnitudes in Figure 3e,f, and peak shifts are therefore compared within rather than across immobilization strategies.

Finally, to evaluate the diagnostic potential of this platform in a clinically relevant setting, measurements were performed in diluted human serum. A four-fold dilution was used to minimize optical turbidity, which hinders UV–vis detection. This turbidity arises predominantly from the largest lipoprotein classes, which are present in adult human serum but largely absent from fetal bovine serum [57]. Here, functionalized nanobiosensors were introduced into serum containing a known concentration of target protein, and the resulting LSPR shift was converted to an apparent concentration by referencing a binding titration curve generated in parallel with the same nanoparticle batch (Figure 4e). The calculated concentration showed good agreement with the known analyte level (PEX52-PEX14: 500 nM vs. 1.4 μM; PEX51-PEX14: 300 nM vs. 270 nM (Figure 4f,g), demonstrating quantitative protein detection in a complex biological fluid for both bioconjugation methods (Figure 4f,g). Together, these results show that the overall platform enables quantitative detection of protein–protein interactions, even for small and intrinsically disordered proteins, and remains effective under physiologically relevant, protein-rich conditions.

Comparable inter-assay variability is well documented for established methods in complex biological matrices where coefficients of variation of 15%–30% are commonly reported for BCA and ELISA, and 11%–26% for antibody-based serum protein quantification even after normalization [58–60]. The spread observed in our datasets falls within this range, indicating that the quantitative precision of our platform in serum is comparable to that of established clinical quantification methods.

We note that quantitative analyte recovery in human serum is subject to several sources of variability absent from the buffer- and FBS-based measurements (Figures 3a,b and 4a,b; Figure S21). Unlike measurements in buffer and FBS, human serum required dilution, and yet residual scattering still resulted in optical backgrounds that differed between independently prepared aliquots of the same stock. The accuracy of the extracted shift is therefore limited more by the optical quality and heterogeneity of the matrix, which must be optimized and calibrated prior to clinical deployment in the future.

3 | Conclusion

In this work, we introduce a solution-phase nanoparticle optical biosensing platform that enables quantitative, real-time analysis of challenging protein-protein interactions directly within complex biological media. Exploiting the versatility of solid-phase peptide synthesis, we employ sequence-defined CysPoly(AEEA) ligands that integrate three functionalities—surface anchoring, antifouling, and site-specific bioconjugation—within a single molecular construct. These ligands substantially reduce non-specific protein adsorption and enable modular, covalent, and site-specific bioconjugation via click chemistry and enzymatic ligation. The subsequent nanobiosensors can reliably detect and quantify specific protein-protein interactions in buffer and

sample (orange). PEX14 was detected in four-fold diluted human serum using PEX5-functionalized sensors prepared via SPAAC (f) or SML (g); calibration curves (red) quantified PEX14 (orange) at 500 nM (SPAAC) and 300 nM (SML). Uncertainties represent the standard error of the mean ($n = 3$) propagated through the inverse Hill–Waud calibration function. For PEX5–PEX14, panels (c,d) show the complementary PEX5 construct to (a,b): PEX51 via SPAAC in (c), PEX52 via SML in (d), confirming that both constructs are compatible with either conjugation strategy.

16136829, 0, Downloaded from https://onlinelibrary.wiley.com/doi/10.1002/smll.75794, Wiley Online Library on [09/11/2026]. See the Terms and Conditions (https://onlinelibrary.wiley.com/terms-and-conditions) on Wiley Online Library for rules of use; OA articles are governed by the applicable Creative Commons License

serum with good agreement with literature values without compromising colloidal stability. The platform is straightforward to operate, does not require expensive or unique instrumentation, and is compatible with common buffers as well as human and animal serum. The modular conjugation chemistry makes the platform readily adaptable to a broad range of protein targets and interaction systems.

Our platform retains robust performance in complex biological environments, delivering selective and detectable responses for multiple intrinsically disordered protein pairs in undiluted serum. Even in diluted human serum, target analytes at known concentrations were recovered through binding titration curves, demonstrating the diagnostic potential of this approach, while indicating that matrix-related optical variability remains to be addressed for quantitative clinical applications.

Although we have demonstrated nanosensor functionality across multiple PPI pairs and environments, we note that performance is still likely protein-dependent, as the physicochemical properties of the immobilized protein can influence nonspecific adsorption. As such, the full breadth of nanosensor compatibility with other proteins remains to be determined and likely requires optimization for each protein pair and media. Nevertheless, the combination of an antifouling CysPoly(AEEA) hybrid ligand interface with versatile covalent conjugation strategies provides a broadly applicable framework for diagnostics and biomolecular interaction studies under physiologically relevant conditions.

4 | Experimental Section/Methods

For methods, experimental details, and supplementary data and figures, please see the Supporting Information.

4.1 | Statistical Analysis

Descriptions of sample sizes, markers, and error bars are included in the figure legends. No statistical tests were performed in this study.

Author Contributions

JC, GA, and MRS conceptualized the project. GA and MRS performed nanoparticle synthesis. GA performed Sortase-mediated ligation, and MRS performed click chemistry reactions. HB and OP synthesized peptide-AEEA hybrids. PZ and MS suggested Sortase-mediated ligation and synthesized recombinant proteins. GA and MRS performed nanoparticle surface chemistry and optical measurements. NS and AW performed MALDI-TOF. NH and MZ performed all-atom molecular dynamics calculations. GA, MRS, and JC wrote the manuscript with input from all authors. JC supervised the project.

Acknowledgements

We gratefully acknowledge funding from Helmholtz Munich. We thank Vladimir Kitaev for assistance with the transferring of protocols for synthesis of silver decahedral nanoparticles and Jacob Speers for preparing samples of decahedra for evaluation and comparison. We also thank Parth Bhuva and Beibei Hao for help with nanoparticle synthesis and Julian Samberger for design and engineering of the home-built nanoparticle photoreactor. The authors used artificial intelligence tools, including OpenAI ChatGPT, Anthropic Claude, and Google Gemini, to assist with text proofreading and to provide language suggestions during the preparation of this manuscript. All content was reviewed and approved by the authors.

Open access funding enabled and organized by Projekt DEAL.

Conflicts of Interest

G.A., M.R.S., H.L.B., P.Z., M.S., O.P., and J.C. are inventors on a patent application regarding the technology presented in this study (EP26214292).

Data Availability Statement

All raw data for the figures presented in this study are available upon reasonable request to the corresponding author.

References

1. J. Westermarck, J. Ivaska, and G. L. Corthals, "Identification of Protein Interactions Involved in Cellular Signaling," *Molecular & Cellular Proteomics* 12 (2013): 1752–1763.

2. J. F. Greenblatt, B. M. Alberts, and N. J. Krogan, "Discovery and Significance of Protein-protein Interactions in Health and Disease," *Cell* 187 (2024): 6501–6517.

3. H. Lu, Q. Zhou, J. He, et al., "Recent Advances in the Development of Protein–Protein Interactions Modulators: Mechanisms and Clinical Trials," *Signal Transduction and Targeted Therapy* 5 (2020): 213.

4. J. F. Rusling and R. J. Forster, "Biosensors Designed for Clinical Applications," *Biomedicines* 9 (2021): 702.

5. A. K. Singh, M. Anwar, R. Pradhan, M. S. Ashar, N. Rai, and S. Dey, "Surface Plasmon Resonance Based-Optical Biosensor: Emerging Diagnostic Tool For Early Detection of Diseases," *Journal of Biophotonics* 16 (2023): 202200380.

6. J. Homola, "Surface Plasmon Resonance Sensors for Detection of Chemical and Biological Species," *Chemical Reviews* 108 (2008): 462–493.

7. E. Mauriz, "Low-Fouling Substrates for Plasmonic Sensing of Circulating Biomarkers in Biological Fluids," *Biosensors* 10 (2020): 63.

8. Y. Tang, X. Zeng, and J. Liang, "Surface Plasmon Resonance: An Introduction to a Surface Spectroscopy Technique," *Journal of Chemical Education* 87 (2010): 742–746.

9. D. Wang, H. Wu, and D. K. Schwartz, "Three-dimensional Tracking of Interfacial Hopping Diffusion," *Physical Review Letters* 119 (2017): 268001.

10. P. Schuck and H. Zhao, "The Role of Mass Transport Limitation and Surface Heterogeneity in the Biophysical Characterization of Macromolecular Binding Processes by SPR Biosensing," *Methods in Molecular Biology* 627 (2010): 15–54.

11. D. Prozeller, S. Morsbach, and K. Landfester, "Isothermal Titration Calorimetry as a Complementary Method for Investigating Nanoparticle–Protein Interactions," *Nanoscale* 11 (2019): 19265–19273.

12. F. Soltermann, W. B. Struwe, and P. Kukura, "Label-Free Methods for Optical In Vitro Characterization of Protein–Protein Interactions," *Physical Chemistry Chemical Physics* 23 (2021): 16488–16500.

13. J. A. Purslow, B. Khatiwada, M. J. Bayro, and V. Venditti, "NMR Methods for Structural Characterization of Protein-protein Complexes," *Frontiers in Molecular Biosciences* 7 (2020): 9.

14. V. Kamat and A. Rafique, "Designing Binding Kinetic Assay on the Bio-layer Interferometry (BLI) Biosensor to Characterize Antibody-antigen Interactions," *Analytical Biochemistry* 536 (2017): 16–31.

15. H.-J. Wu, J. Henzie, W.-C. Lin, et al., "Membrane-protein Binding Measured With Solution-phase Plasmonic Nanocube Sensors," *Nature Methods* 9 (2012): 1189–1191.

16136829, 0, Downloaded from https://onlinelibrary.wiley.com/doi/10.1002/smll.75794, Wiley Online Library on [09/11/2026]. See the Terms and Conditions (https://onlinelibrary.wiley.com/terms-and-conditions) on Wiley Online Library for rules of use; OA articles are governed by the applicable Creative Commons License

16. J. Zhou, K. Ridderbeek, P. Zou, et al., "Modular Nanoparticle Platform for Solution-Phase Optical Sensing of Protein–Protein Interactions," *ACS Applied Optical Materials* 3 (2025): 676–688.

17. A. B. Taylor and P. Zijlstra, "Single-Molecule Plasmon Sensing: Current Status and Future Prospects," *ACS Sensors* 2 (2017): 1103–1122.

18. K. M. Mayer and J. H. Hafner, "Localized Surface Plasmon Resonance Sensors," *Chemical Reviews* 111 (2011): 3828–3857.

19. R. García-Álvarez and M. Vallet-Regí, "Hard and Soft Protein Corona of Nanomaterials: Analysis and Relevance," *Nanomaterials* 11 (2021): 888.

20. S. Cheeseman, P. Moazzam, N. Mahmoudi, et al., "The Challenges and Opportunities of Protein Coronas for Nanoscale Biomolecular Sensing," *Small* 21 (2025): 03820.

21. A. M. C. Maan, A. H. Hofman, W. M. de Vos, and M. Kamperman, "Recent Developments and Practical Feasibility of Polymer-Based Antifouling Coatings," *Advanced Functional Materials* 30 (2020): 2000936.

22. V. P. Chavda, J. Ajabiya, D. Teli, J. Bojarska, and V. Apostolopoulos, "Tirzepatide, a New Era of Dual-targeted Treatment for Diabetes and Obesity: A Mini-review," *Molecules* 27 (2022): 4315.

23. P. Jolly, M. R. Batistuti, A. Miodek, et al., "Highly Sensitive Dual Mode Electrochemical Platform for microRNA Detection," *Scientific Reports* 6 (2016): 36719.

24. U. Tsylents, I. Siekierska, and J. Trylska, "Peptide Nucleic Acid Conjugates and Their Antimicrobial Applications—A Mini-Review," *European Biophysics Journal* 52 (2023): 533–544.

25. M. Shi, Y. Li, W. Wang, R. Han, and X. Luo, "A Super-antifouling Electrochemical Biosensor for Protein Detection in Complex Biofluids Based on PEGylated Multifunctional Peptide," *ACS Sensors* 9 (2024): 2956–2963.

26. B. Simões, W. J. Guedens, C. Keene, et al., "Direct Immobilization of Engineered Nanobodies on Gold Sensors," *ACS Appl Mater Interfaces* 13 (2021): 17353–17360.

27. N. J. Agard, J. A. Prescher, and C. R. Bertozzi, "A Strain-Promoted [3 + 2] Azide–Alkyne Cycloaddition for Covalent Modification of Biomolecules in Living Systems," *Journal of the American Chemical Society* 126 (2004): 15046–15047.

28. H. Mao, S. A. Hart, A. Schink, and B. A. Pollok, "Sortase-Mediated Protein Ligation: A New Method for Protein Engineering," *Journal of the American Chemical Society* 126 (2004): 2670–2671.

29. R. J. A. Wanders, M. Baes, D. Ribeiro, S. Ferdinandusse, and H. R. Waterham, "The Physiological Functions of human Peroxisomes," *Physiological Reviews* 103 (2023): 957–1024.

30. T. Cedervall, I. Lynch, S. Lindman, et al., "Understanding the Nanoparticle–Protein Corona Using Methods to Quantify Exchange Rates and Affinities of Proteins for Nanoparticles," *Proceedings of the National Academy of Sciences* 104 (2007): 2050–2055.

31. V. Jagalski, R. D. Barker, M. B. Thygesen, et al., "Grafted Biomembranes Containing Membrane Proteins—the Case of the Leucine Transporter," *Soft Matter* 11 (2015): 7707–7711.

32. M. Lundqvist, J. Stigler, G. Elia, I. Lynch, T. Cedervall, and K. A. Dawson, "Nanoparticle Size and Surface Properties Determine the Protein Corona With Possible Implications for Biological Impacts," *Proceedings of the National Academy of Sciences* 105 (2008): 14265–14270.

33. H. Mohammad-Beigi, Y. Hayashi, C. M. Zeuthen, et al., "Mapping and Identification of Soft Corona Proteins at Nanoparticles and Their Impact on Cellular Association," *Nature Communications* 11 (2020): 4535.

34. D. Baimanov, J. Wang, J. Zhang, et al., "In Situ Analysis of Nanoparticle Soft Corona and Dynamic Evolution," *Nature Communications* 13 (2022): 5389.

35. C. A. Del Grosso, C. Leng, K. Zhang, et al., "Surface Hydration for Antifouling and Bio-Adhesion," *Chemical Science* 11 (2020): 10367–10377.

36. J. L. Hanigan-Diebel, R. J. Costin, L. C. Myers, et al., "Affinity Constants of Bovine Serum Albumin for 5 Nm Gold Nanoparticles (AuNPs) With ω-functionalized Thiol Monolayers Determined by Fluorescence Spectroscopy," *Langmuir* 40 (2024): 15558–15568.

37. N. Türkel, "Stability Constants of Mixed Ligand Complexes of Nickel(II) With Adenine and Some Amino Acids," *Bioinorganic Chemistry and Applications* 2015 (2015): 1–9.

38. Z. S. Hendsch and B. Tidor, "Do Salt Bridges Stabilize Proteins? A Continuum Electrostatic Analysis," *Protein Science* 3 (1994): 211–226.

39. C. N. Pace, H. Fu, K. L. Fryar, et al., "Contribution of Hydrogen Bonds to Protein Stability," *Protein Science* 23 (2014): 652–661.

40. K. Renault, J. W. Fredy, P.-Y. Renard, and C. Sabot, "Covalent Modification of Biomolecules Through Maleimide-Based Labeling Strategies," *Bioconjugate Chemistry* 29 (2018): 2497–2513.

41. D. Svatunek, N. Houszka, T. A. Hamlin, F. M. Bickelhaupt, and H. Mikula, "Chemoselectivity of Tertiary Azides in Strain-Promoted Alkyne-Azide Cycloadditions," *Chemistry—A European Journal* 25 (2019): 754–758.

42. S. Pritz, Y. Wolf, O. Kraetke, J. Klose, M. Bienert, and M. Beyermann, "Synthesis of Biologically Active Peptide Nucleic Acid–Peptide Conjugates by Sortase-Mediated Ligation," *The Journal of Organic Chemistry* 72 (2007): 3909–3912.

43. J. Li, Y. Zhang, O. Soubias, et al., "Optimization of Sortase A Ligation for Flexible Engineering of Complex Protein Systems," *Journal of Biological Chemistry* 295 (2020): 2664–2675.

44. J. Idiago-López, E. Moreno-Antolín, M. Eceiza, et al., "From Bench to Cell: A Roadmap for Assessing the Bioorthogonal "Click" Reactivity of Magnetic Nanoparticles for Cell Surface Engineering," *Bioconjugate Chemistry* 33 (2022): 1620–1633.

45. L. Chan, H. F. Cross, J. K. She, G. Cavalli, H. F. P. Martins, and C. Neylon, "Covalent Attachment of Proteins to Solid Supports and Surfaces via Sortase-mediated Ligation," *PLoS ONE* 2 (2007): 1164.

46. Q. Dai, C. Walkey, and W. C. W. Chan, "Polyethylene Glycol Backfilling Mitigates the Negative Impact of the Protein Corona on Nanoparticle Cell Targeting," *Angewandte Chemie International Edition* 53 (2014): 5093–5096.

47. J. Beurton, P. Lavalle, A. Pallotta, T. Chaigneau, I. Clarot, and A. Boudier, "Design of Surface Ligands for Blood Compatible Gold Nanoparticles: Effect of Charge and Binding Energy," *International Journal of Pharmaceutics* 580 (2020): 119244.

48. S. M. Marinakos, S. Chen, and A. Chilkoti, "Plasmonic Detection of a Model Analyte in Serum by a Gold Nanorod Sensor," *Analytical Chemistry* 79 (2007): 5278–5283.

49. V. Voisin, J. Pilate, P. Damman, P. Mégret, and C. Caucheteur, "Highly Sensitive Detection of Molecular Interactions With Plasmonic Optical Fiber Grating Sensors," *Biosensors and Bioelectronics* 51 (2014): 249–254.

50. M. Focsan, A. Campu, A.-M. Craciun, et al., "A Simple and Efficient Design to Improve the Detection of Biotin-streptavidin Interaction With Plasmonic Nanobiosensors," *Biosensors and Bioelectronics* 86 (2016): 728–735.

51. X. Li, L. Jiang, Q. Zhan, J. Qian, and S. He, "Localized Surface Plasmon Resonance (LSPR) of Polyelectrolyte-functionalized Gold-nanoparticles for Bio-sensing," *Colloids and Surfaces A: Physicochemical and Engineering Aspects* 332 (2009): 172–179.

52. M. Gopalswamy, C. Zheng, S. Gaussmann, et al., "Distinct Conformational and Energetic Features Define the Specific Recognition of (di)Aromatic Peptide Motifs by PEX14," *Biological Chemistry* 404 (2023): 179–194.

53. A. Neuhaus, H. Kooshapur, J. Wolf, et al., "A Novel Pex14 Protein-interacting Site of human Pex5 Is Critical for Matrix Protein Import Into Peroxisomes," *Journal of Biological Chemistry* 289 (2014): 437–448.

16136829, 0, Downloaded from https://onlinelibrary.wiley.com/doi/10.1002/smll.75794, Wiley Online Library on [09/11/2026]. See the Terms and Conditions (https://onlinelibrary.wiley.com/terms-and-conditions) on Wiley Online Library for rules of use; OA articles are governed by the applicable Creative Commons License

54. J. Wang, H. N. Do, K. Koirala, and Y. Miao, "Predicting Biomolecular Binding Kinetics: A Review," *Journal of Chemical Theory and Computation* 19 (2023): 2135–2148.

55. C. W. Lee, M. A. Martinez-Yamout, H. J. Dyson, and P. E. Wright, "Structure of the p53 Transactivation Domain in Complex With the Nuclear Receptor Coactivator Binding Domain of CREB Binding Protein," *Biochemistry* 49 (2010): 9964–9971.

56. S. Gaussmann, M. Gopalswamy, M. Eberhardt, et al., "Membrane Interactions of the Peroxisomal Proteins PEX5 and PEX14," *Frontiers in Cell and Developmental Biology* 9 (2021): 651449.

57. C.-J. L. Farrell and A. C. Carter, "Serum Indices: Managing Assay Interference," *Annals of Clinical Biochemistry: International Journal of Laboratory Medicine* 53 (2016): 527–538.

58. E. Rogatsky, "Pandora Box of BCA Assay. Investigation of the Accuracy and Linearity of the Microplate Bicinchoninic Protein Assay: Analytical Challenges and Method Modifications to Minimize Systematic Errors," *Analytical Biochemistry* 631 (2021): 114321.

59. S. Aydin, E. Emre, K. Ugur, et al., "An Overview of ELISA: A Review and Update on Best Laboratory Practices for Quantifying Peptides and Proteins in Biological Fluids," *Journal of International Medical Research* 53 (2025): 3000605251315913.

60. T. D. Christensen, E. Maag, K. Madsen, S. C. Lindgaard, D. L. Nielsen, and J. S. Johansen, "Determination of Temporal Reproducibility and Variability of Cancer Biomarkers in Serum and EDTA Plasma Samples Using a Proximity Extension Assay," *Clinical Proteomics* 19 (2022): 39.

Supporting Information

Additional supporting information can be found online in the Supporting Information section.

Supporting File: smll75794-sup-0001-SuppMat.pdf.

16136829, 0, Downloaded from https://onlinelibrary.wiley.com/doi/10.1002/smll.75794, Wiley Online Library on [09/11/2026]. See the Terms and Conditions (https://onlinelibrary.wiley.com/terms-and-conditions) on Wiley Online Library for rules of use; OA articles are governed by the applicable Creative Commons License